scientific reports

OPEN

Endoplasmic reticulum stress sensor protein PERK in hepatic stellate cells promotes the progression of hepatocellular carcinoma via p38δ MAPK/IL-1β axis

Makoto Morita, Yoshio Tokumoto✉, Takao Watanabe, Yusuke Imai, Atsushi Yukimoto, Toyoki Shimamoto, Ryo Yano, Yuki Okazaki, Yoshiko Nakamura, Osamu Yoshida, Teruki Miyake, Masashi Hirooka, Masanori Abe & Yoichi Hiasa

Palmitic acid (PA) absorption from the intestine is increased in metabolic dysfunction-associated steatohepatitis (MASH). It induces endoplasmic reticulum (ER) stress and interleukin-1 beta (IL-1β) production in hepatic stellate cells (HSCs). Protein kinase R-like endoplasmic reticulum kinase (PERK) is an ER stress sensor protein involved in HSC activation and liver fibrosis. However, its role in HSCs during hepatocellular carcinoma (HCC) progression remains unclear. This study clarified the process of IL-1β production via PERK in HSCs and explored the mechanism underlying MASH-related HCC progression. HSCs were treated with PA or transfected with PERK small-interfering RNA (siRNA) or PERK plasmid. Proliferation, scratch, and Transwell assays were performed on HCC cells cultured in the conditioned medium (CM) from HSCs. PA treatment increased PERK and IL-1β expression in HSCs. PERK knockdown decreased IL-1β expression, while its overexpression increased it in HSCs. The CM from PA-treated HSCs showed elevated IL-1β levels and enhanced HCC cells' proliferation, migration, and invasion; however, these effects were suppressed by PERK knockdown in HSCs. RNA-sequencing analysis revealed that p38δ mitogen-activated protein kinase (MAPK) is the intermediate molecule between PERK and IL-1β in HSCs. In the tumor microenvironment of MASH-related HCC, PERK in HSCs promotes HCC progression via the p38δ MAPK/IL-1β axis.

Keywords Metabolic dysfunction-associated steatohepatitis, Hepatic stellate cells, Hepatocellular carcinoma, Protein kinase R-like endoplasmic reticulum kinase, Interleukin-1 beta

Despite advancements in chemotherapy, hepatocellular carcinoma (HCC) remains one of the cancers with poor prognosis worldwide[1]. Although most HCC cases have been attributed to hepatitis C and B virus infections, the incidence of HCC resulting from these viral infections is declining owing to developments in antiviral therapies. In contrast, the cases of non-hepatitis B and C-related HCC have been increasing, primarily driven by metabolic dysfunction-associated steatotic liver disease (MASLD) and alcohol-associated liver disease[2]. MASLD cases are rapidly rising worldwide, largely due to the increase in the obese population[3]. Metabolic dysfunction-associated steatohepatitis (MASH), which accounts for 10–20% of MASLD cases, frequently progresses to liver cirrhosis and subsequently develops into HCC. As the number of patients with MASH is projected to increase in the future[4], a rise in MASH-related HCC cases is also expected. Immune checkpoint inhibitors, which are the first-line drugs for treating advanced HCC, have been reported to be less effective in MASH-related HCC cases due to their unique microenvironment[5]. Therefore, elucidating the pathogenesis of MASH-related HCC is imperative for improving HCC prognosis.

Department of Gastroenterology and Metabology, Ehime University Graduate School of Medicine, 454 Shitsukawa, Toon, Ehime 791-0295, Japan. ✉email: tokumoto.yoshio.cc@ehime-u.ac.jp

HCC generates a complex tumor microenvironment (TME)[6] comprising both tumor and non-parenchymal cells[7]. The crosstalk between these tumor and non-parenchymal cells influences tumor progression and response to anticancer therapy[8]. Hepatic stellate cells (HSCs), which are representative non-parenchymal cells, have been reported to affect HCC progression by secreting cytokines and chemokines[9,10]. They store vitamin A and reside in the space of Disse[11,12]. HSCs become activated when exposed to various factors, such as cytokines[13], lipopolysaccharide (LPS)[14], and free fatty acids[15]. Activated HSCs induce liver fibrosis by secreting the extracellular matrix[16]. In MASH, the saturated fatty acids, including palmitic acid (PA), absorbed in the intestinal tract flow into the hepatic sinusoid via the portal vein and have various effects on the hepatic microenvironment[17]. We previously reported that the PA absorption was increased, leading to HSC activation in MASH model rats[18]. PA-treated HSCs were also reported to produce interleukin-1 beta (IL-1β) and promote HCC progression[19]. However, the precise mechanism behind this remains unclear. PA is also known to induce endoplasmic reticulum (ER) stress in human hepatocytes through protein kinase R-like endoplasmic reticulum kinase (PERK) activation[20] and may similarly induce ER stress in HSCs. Although reports are available on ER stress in HSCs, most of them are related to HSC activation and liver fibrosis, and only a few address its role in HCC progression. PERK was also reported to regulate IL-1β production in murine macrophages[21]. Recent studies have demonstrated that ER stress contributes to the epithelial–mesenchymal transition and drug resistance in HCC[22,23], highlighting its importance as a potential therapeutic target. ER stress in HSCs within the TME of MASH-related HCC may affect HCC progression through IL-1β production.

This study aimed to clarify the PERK-mediated IL-1β production pathway in HSCs and the underlying mechanism driving MASH-related HCC progression.

Results

PA activates the PERK signaling pathway and upregulates IL-1β expression

Previous studies have reported that PA induces ER stress in hepatocytes; therefore, we analyzed the expression of PERK and PERK-related molecules in PA-treated HSCs using reverse transcription PCR (RT-PCR) and western blotting (WB). The PERK messenger RNA (mRNA) expression was upregulated (Fig. 1a), and the protein expression of PERK and phosphorylated eukaryotic initiation factor 2-alpha (p-eIF2α) was elevated (Fig. 1b) in PA-treated LX-2 cells. We previously reported that PA promotes IL-1β production in LX-2 cells. In this study, we reconfirmed that PA treatment upregulated the mRNA (Fig. 1c) and protein (Fig. 1d) expression of IL-1β in LX-2 cells.

PERK knockdown with siRNA decreases IL-1β expression

We transfected PERK small-interfering RNA (siRNA) into LX-2 cells to investigate the relationship between PERK and IL-1β in HSCs. RT-PCR (Fig. 2a) and WB (Fig. 2b) confirmed the knockdown of PERK mRNA and protein. The p-eIF2α expression was reduced, and PERK siRNA suppressed PERK signaling in LX-2 cells. Subsequently, we analyzed the mRNA (Fig. 2c) and protein (Fig. 2d) expression of IL-1β in PERK-knockdown LX-2 cells and found that it was decreased. Furthermore, to examine the specific role of PERK in PA-induced IL-1β production, the PERK-knockdown cells were treated with PA. We confirmed that the PA-induced increase in IL-1β expression was suppressed in these cells, as evaluated by RT-PCR (Fig. 2e) and WB (Fig. 2f).

PERK overexpression increases IL-1β expression

We investigated the effect of PERK overexpression on IL-1β expression in HSCs by transfecting the PERK-overexpression plasmid into LX-2 cells and analyzing the PERK mRNA and protein expression. PERK mRNA expression was increased in the PERK plasmid-transfected cells (Fig. 3a). WB confirmed the exogenous green fluorescent protein-tagged PERK, which is 27 kDa larger than the endogenous PERK, and the increase in p-eIF2α expression (Fig. 3b). Furthermore, the mRNA (Fig. 3c) and protein (Fig. 3d) expression of IL-1β was increased in the PERK-overexpressing cells. These results demonstrate that PERK regulates IL-1β expression in HSCs.

IL-1β promotes HCC cell growth

We treated HepG2 cells with recombinant human IL-1β (rhIL-1β) to assess their growth since IL-1β has been reported to promote HCC cell proliferation[19]. The 3-(4,5-dimethylthiazol-2-yl)-5-(3-carboxymethoxyphenyl)-2-(4-sulfophenyl)-2H-tetrazolium (MTS) assay revealed that rhIL-1β promoted the growth of HepG2 cells dose-dependently (Fig. 4a). We examined whether an IL-1β neutralizing antibody (IL-1β NAb) suppressed the growth of HepG2 cells cultured in conditioned medium (CM) from PA-treated LX-2 cells, which exhibit increased IL-1β expression. The growth of HepG2 cells cultured in CM from PA-treated LX-2 cells was dose-dependently attenuated by IL-1β NAb (Fig. 4b). This result suggests that PA-treated LX-2 cells secrete IL-1β, which plays a crucial role in promoting the growth of HepG2 cells. Next, an enzyme-linked immunosorbent assay (ELISA) was performed to confirm the extracellular secretion of IL-1β from LX-2 cells. We measured the IL-1β concentration in CM from control siRNA- or PERK siRNA-transfected LX-2 cells treated with bovine serum albumin (BSA) or PA. The IL-1β concentration in CM from PA-treated LX-2 cells was higher than that in CM from BSA-treated LX-2 cells; however, PERK knockdown in PA-treated LX-2 cells suppressed IL-1β secretion (Fig. 4c). To evaluate the effect of CM from PA-treated LX-2 cells on the growth of HepG2 cells, we used CM from LX-2 cells under different conditions. The growth of HepG2 cells was enhanced when cultured in CM from PA-treated LX-2 cells compared to that from BSA-treated LX-2 cells. However, the promotion of HepG2 cell growth by CM from PA-treated LX-2 cells was suppressed by PERK knockdown in LX-2 cells (Fig. 4d). These results show that HSCs exposed to PA promote HCC cell growth by enhancing IL-1β secretion via PERK.
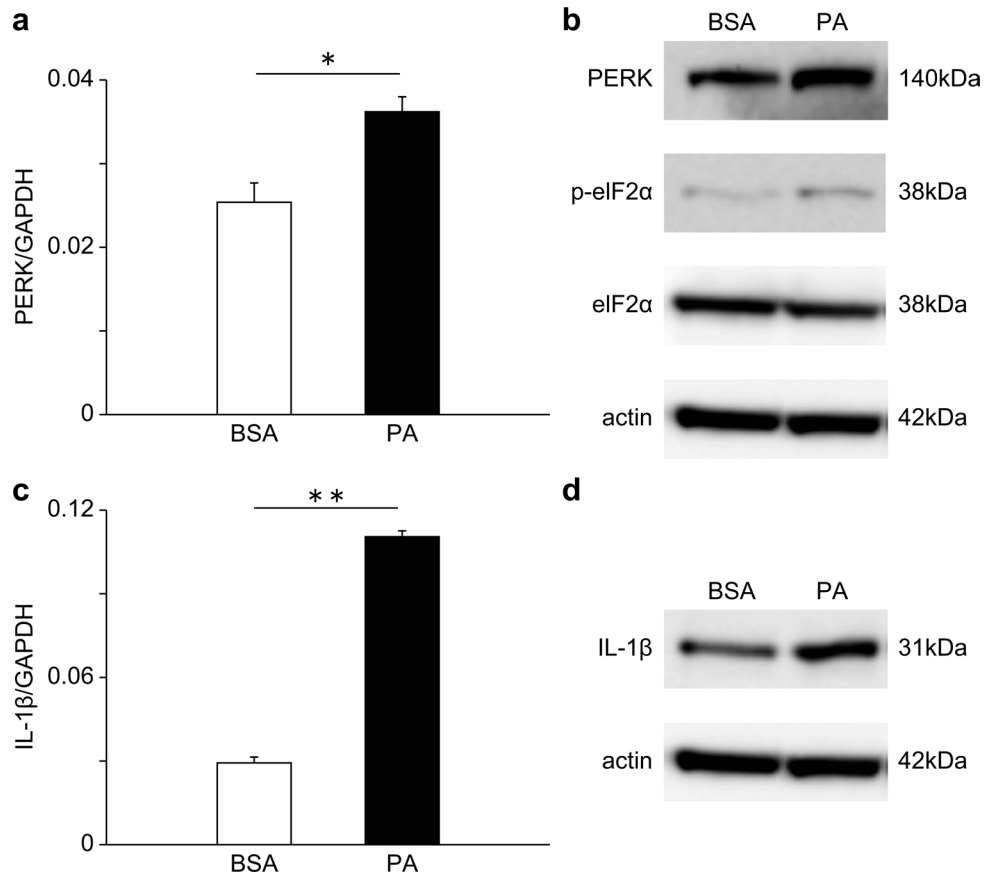
Fig. 1. PA activates the PERK signaling pathway and increases IL-1β expression in HSCs. LX-2 cells are treated with BSA or PA (20 μM), and the expression of PERK, downstream molecules of PERK, and IL-1β is examined. (**a**) PERK mRNA expression is evaluated using RT-PCR (n = 4). (**b**) Protein expression of PERK, p-eIF2α, and eIF2α is determined using WB. Supplementary Fig. S1 shows the original membranes of WB. IL-1β mRNA (**c**) and protein (**d**) expression are evaluated using RT-PCR (n = 4) and WB, respectively. Supplementary Fig. S2 presents the original membranes of WB. Data are shown as the mean ± SE. Statistical analysis is performed using Student's *t*-test. *$p < 0.05$, **$p < 0.01$. *Abbreviations*: PERK, Protein kinase R-like endoplasmic reticulum kinase; IL-1β, Interleukin-1 beta; GAPDH, Glyceraldehyde 3-phosphate dehydrogenase; WB, Western blotting; RT, Reverse transcription; siRNA, Small-interfering RNA; HSCs, Hepatic stellate cells; SE, Standard error; PA, Palmitic acid; BSA, Bovine serum albumin; p-eIF2α, Phosphorylated eukaryotic initiation factor 2-alpha.

HSCs treated with PA enhance HCC cell migration and invasion

Since IL-1β has been reported to promote HCC cell migration and invasion[24], we performed scratch and Transwell assays to determine whether CM from PA-treated HSCs enhances HCC cell migration and invasion. The scratch assay showed that CM from PA-treated LX-2 cells enhanced HepG2 cell migration; however, this effect was suppressed by PERK knockdown in LX-2 cells (Fig. 5a). Similarly, the Transwell assay revealed that CM from PA-treated LX-2 cells promoted HepG2 cell migration and invasion, but PERK knockdown suppressed these effects in LX-2 cells (Fig. 5b and c). These findings suggest that HSCs exposed to PA induce IL-1β production via PERK, thereby promoting HCC cell migration and invasion.

p38δ MAPK mediates the signaling between PERK and IL-1β

We established that PERK promotes IL-1β secretion in HSCs and enhances the malignant behaviors of HCC; however, the mechanism by which IL-1β is induced remains unclear. Therefore, RNA-seq analysis was conducted to identify the molecule that mediates the signaling between PERK and IL-1β. The differentially expressed genes (DEGs) in PA-treated LX-2 cells and PERK siRNA-transfected PA-treated LX-2 cells were visualized using the heatmap (Fig. 6a). We extracted the genes that have been reported to be associated with IL-1β among the DEGs between PA-treated LX-2 cells and PERK siRNA-transfected PA-treated LX-2 cells (Supplementary Table S1). Among them, we focused on *MAPK13* (p38δ MAPK), which encodes a cytoplasmic protein and is associated with inflammatory cytokines production[25] and tumor growth[26]. The volcano plots showed that *EIF2AK3* (PERK), *IL1B* (IL-1β), and *MAPK13* (p38δ MAPK) were markedly downregulated by PERK knockdown (Fig. 6b). To investigate whether modulating PERK expression affects p38δ MAPK expression, we analyzed p38δ MAPK expression in LX-2 cells transfected with PERK siRNA or PERK plasmid using RT-PCR and WB. The mRNA and protein expression of p38δ MAPK was decreased and increased in the PERK-knockdown (Fig. 6c and d)
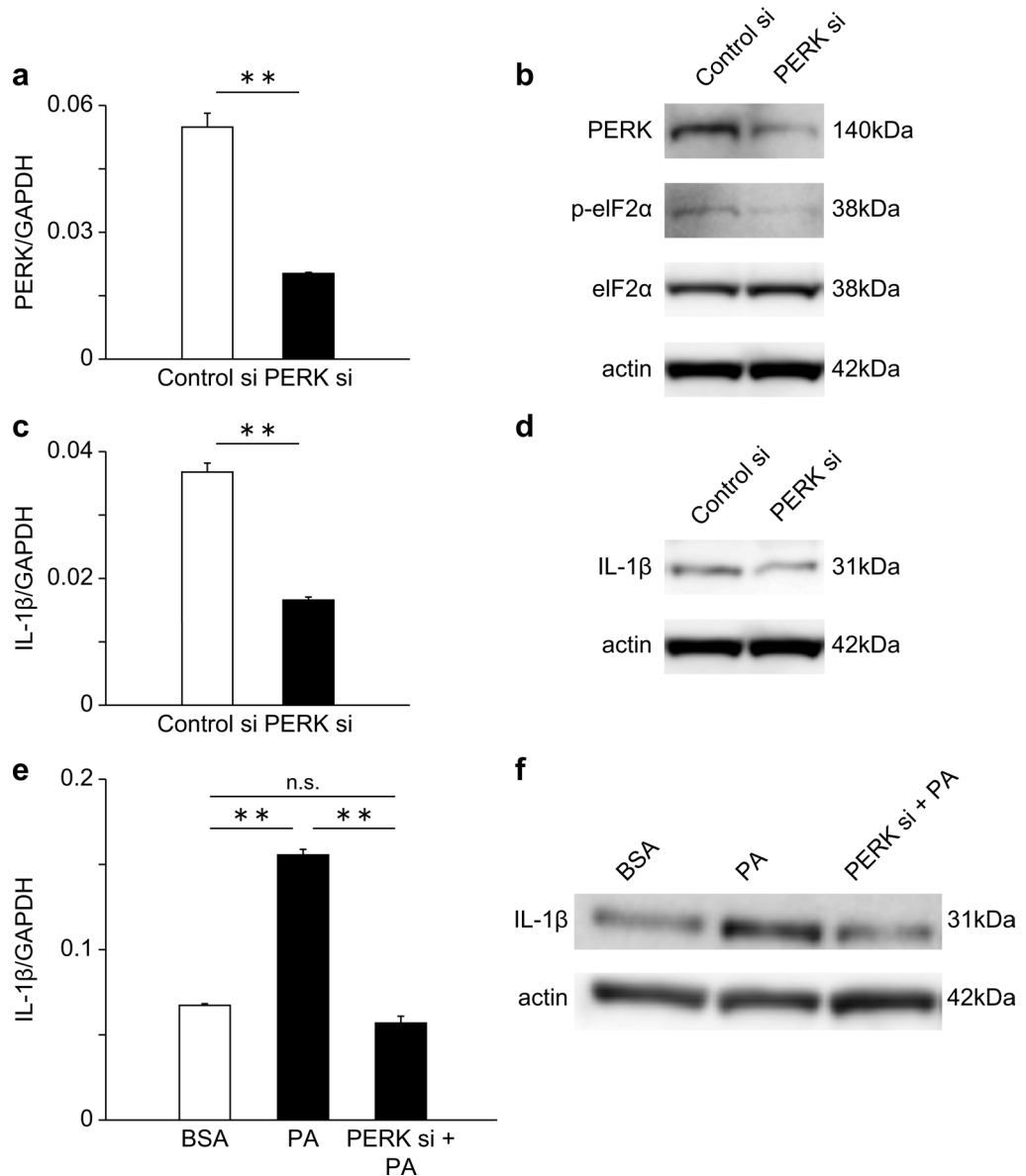
Fig. 2. PERK knockdown suppresses IL-1β expression in HSCs. PERK is knocked down in LX-2 cells using siRNA, and the expression of PERK, downstream molecules of PERK, and IL-1β is examined. (**a**) PERK mRNA expression is evaluated using RT-PCR (n = 4). (**b**) Protein expression of PERK, p-eIF2α, and eIF2α is determined using WB. Supplementary Fig. S3 presents the original membranes of WB. IL-1β mRNA (**c**) and protein (**d**) expression are evaluated using RT-PCR (n = 4) and WB, respectively. Supplementary Fig. S4 shows the original membranes of WB. PERK-knockdown cells are treated with PA, and the change in IL-1β expression is verified. (**e**) IL-1β mRNA (**e**) and protein (**f**) expression are evaluated using RT-PCR (n = 4) and WB, respectively. Supplementary Fig. S5 presents the original membranes of WB. Data are shown as the mean ± SE. Statistical analysis is performed using Student's *t*-test or one-way ANOVA followed by Tukey's multiple comparison test. *******p* < 0.01. *Abbreviations*: PERK, protein kinase R-like endoplasmic reticulum kinase; IL-1β, interleukin-1 beta; GAPDH, glyceraldehyde 3-phosphate dehydrogenase; WB, western blotting; RT, reverse transcription; siRNA, small interfering RNA; HSCs, hepatic stellate cells; SE, standard error; PA, palmitic acid; BSA, bovine serum albumin; ANOVA, analysis of variance; p-eIF2α, phosphorylated eukaryotic initiation factor 2-alpha; n.s., not significant.

and PERK-overexpressing (Fig. 6e and f) cells, respectively. Subsequently, p38δ MAPK siRNA was transfected into LX-2 cells to investigate whether p38δ MAPK regulates IL-1β expression. The knockdown of p38δ MAPK mRNA and protein was confirmed using RT-PCR and WB (Fig. 7a and b). We analyzed the mRNA and protein expression of IL-1β in p38δ MAPK siRNA-transfected LX-2 cells and found that it was downregulated in the p38δ MAPK-knockdown cells (Fig. 7a and b). Furthermore, p38δ MAPK overexpression plasmid was transfected into LX-2 cells to determine whether p38δ MAPK overexpression induces IL-1β upregulation. The result showed that p38δ MAPK mRNA expression was increased in the p38δ MAPK plasmid-transfected LX-2 cells (Fig. 7c).

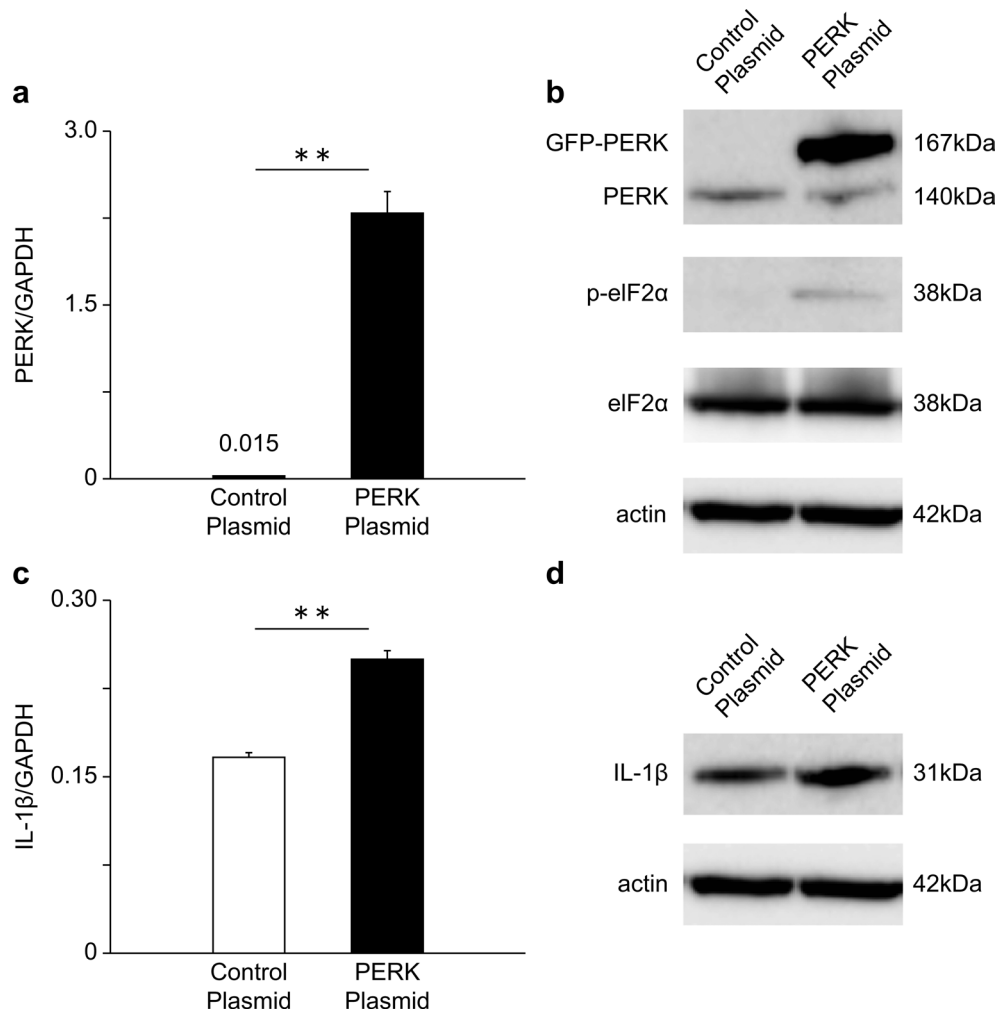**Fig. 3**. PERK overexpression increases IL-1β expression in HSCs. PERK is overexpressed in LX-2 cells using a plasmid, and the expression of PERK, downstream molecules of PERK, and IL-1β is examined. (**a**) PERK mRNA expression is evaluated using RT-PCR (n = 4). (**b**) The expression of GFP-PERK, PERK, p-eIF2α, and eIF2α is determined using WB. Supplementary Fig. S6 presents the original membranes of WB. (**c**) IL-1β mRNA expression is evaluated by RT-PCR (n = 4). (**d**) IL-1β protein expression is determined using WB. Supplementary Fig. S7 presents the original membranes of WB. Data are shown as the mean ± SE. Statistical analysis is performed using Student's t-test. **$p < 0.01$. *Abbreviations*: PERK, Protein kinase R-like endoplasmic reticulum kinase; IL-1β, Interleukin-1 beta; GAPDH, Glyceraldehyde 3-phosphate dehydrogenase; WB, Western blotting; RT, Reverse transcription; siRNA, Small interfering RNA; HSCs, Hepatic stellate cells; SE, Standard error; GFP, Green fluorescent protein; p-eIF2α, Phosphorylated eukaryotic initiation factor 2-alpha.

WB confirmed the expression of exogenous Myc-DDK-tagged p38δ MAPK, which is approximately 2 kDa larger than the endogenous p38δ MAPK (Fig. 7d). Furthermore, the mRNA and protein expression of IL-1β was upregulated in the p38δ MAPK-overexpressing cells (Fig. 7c and d). These results demonstrate that LX-2 cells produce IL-1β via the PERK/p38δ MAPK axis.

Discussion

In the present study, ER stress-induced HSCs were found to increase IL-1β production via PERK and enhance the abilities of HCC cells to proliferate, migrate, and invade. We also revealed that p38δ MAPK mediates the signaling between PERK and IL-1β in HSCs. Several reports have recently demonstrated that HSCs promote HCC progression by secreting various biological contents[27]. We previously demonstrated that LPS- or PA-treated HSCs increase the growth and invasion abilities of HCC cells through IL-1β production following protein kinase R activation. In this study, we revealed that PERK also promotes IL-1β production in HSCs.

PERK is one of the transmembrane proteins in ER that sense misfolded proteins. It activates eIF2α and regulates its downstream targets once ER stress is induced. In chronic liver disease, ER stress is induced by various factors, such as hepatitis viruses, alcohol, and a high-fat diet, and it contributes to disease progression and HCC pathogenesis[28]. Previous reports have demonstrated that ER stress induces HSC activation and liver fibrosis[29–31]. Inositol-requiring enzyme 1α, an ER stress sensor protein, has been reported to be involved in HCC
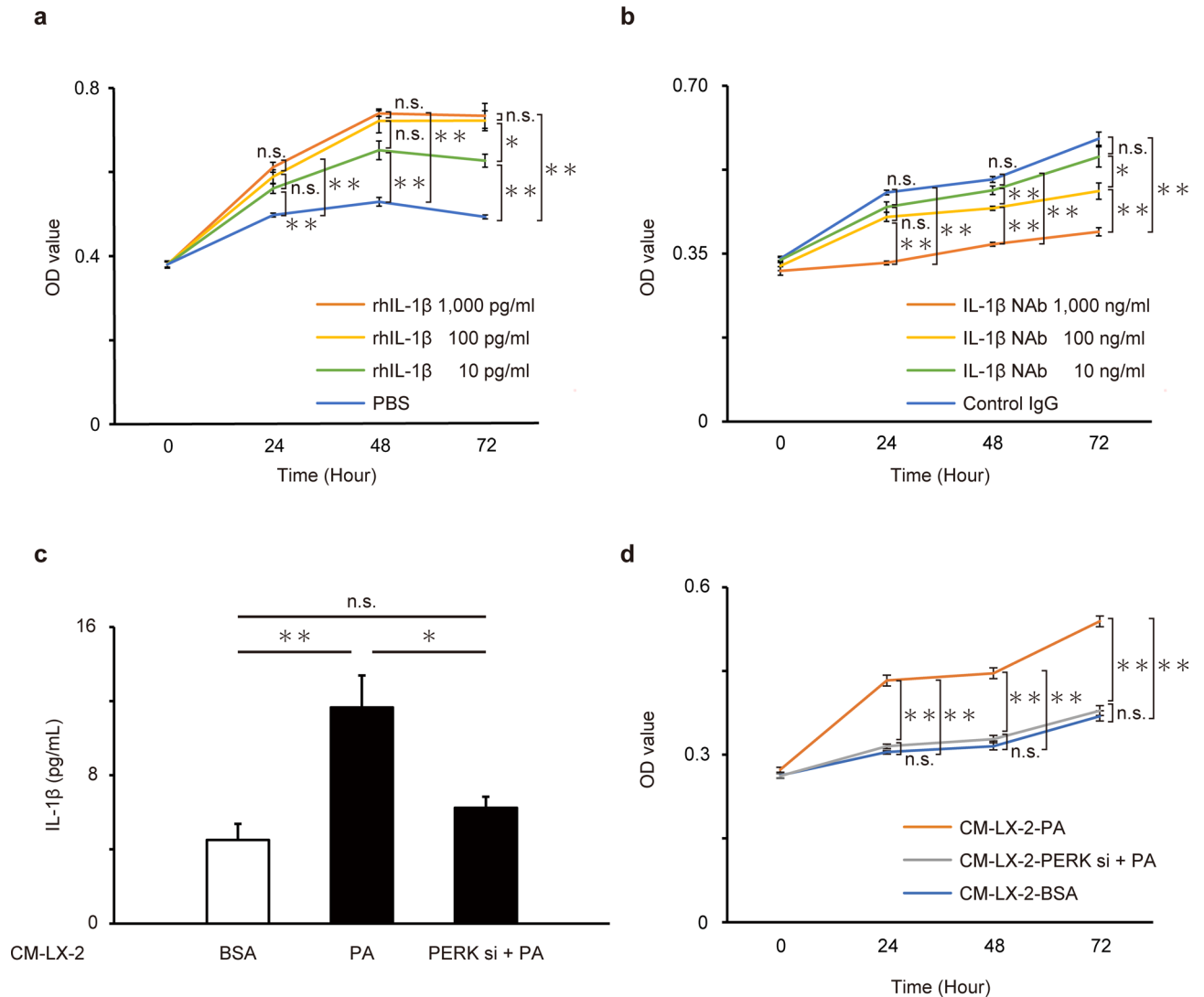
Fig. 4. IL-1β promotes HCC cell growth. (**a**) HepG2 cell growth following rhIL-1β treatment is assessed by MTS assay (n = 6). (**b**) The effect of an IL-1β NAb on HepG2 cell growth cultured in CM from PA-treated LX-2 cells is examined using MTS assay (n = 6). Conditioned media from BSA-treated, PA-treated, and PERK siRNA-transfected PA-treated LX-2 cells are used to examine the effect of HSCs on HCC cell growth. (**c**) IL-1β concentration in each CM is measured using ELISA (n = 4). (**d**) HepG2 cell growth cultured in each CM is verified using MTS assay (n = 6). Data are shown as the mean ± SE. Statistical analysis is performed using one-way ANOVA followed by Tukey's multiple comparison test. *$p < 0.05$, **$p < 0.01$. *Abbreviations*: PERK, protein kinase R-like endoplasmic reticulum kinase; IL-1β, interleukin-1 beta; siRNA, small interfering RNA; HSCs, hepatic stellate cells; SE, standard error; PA, palmitic acid; ANOVA, analysis of variance; BSA, bovine serum albumin; CM, conditioned medium; HCC, hepatocellular carcinoma; ELISA, enzyme-linked immunosorbent assay; MTS, 3-(4,5-dimethylthiazol-2-yl)-5-(3-carboxymethoxyphenyl)-2-(4-sulfophenyl)-2H-tetrazolium; OD, optical density; n.s., not significant; rhIL-1β, recombinant human interleukin-1 beta; IL-1β Nab, interleukin-1 beta neutralizing antibody.

progression[32]. However, no reports exist on the role of PERK in HSCs and HCC progression. Therefore, we examined whether PERK in HSCs influences HCC progression and demonstrated that PERK enhances IL-1β production via p38δ MAPK, contributing to HCC progression.

p38δ MAPK is an isoform of p38 MAPK that functions in extracellular stimuli-induced cellular responses. It has been shown to upregulate the expression of IL-1β and tumor necrosis factor-alpha, which are closely involved in inflammatory responses[33]. Among the four p38 MAPK isoforms, p38α MAPK is the most abundantly expressed in various tissues, making it the primary focus of most research. Although p38α MAPK was considered a potential drug target, p38α MAPK-deficient mice showed embryonic lethality, highlighting the essential roles of p38α MAPK in growth and development[34]. Compared to p38α MAPK, p38δ MAPK is not abundantly expressed in all tissues and exhibits tissue-specific expression, such as in the endocrine glands and small intestine[35]. Therefore, p38δ MAPK has not received considerable attention. However, p38δ MAPK
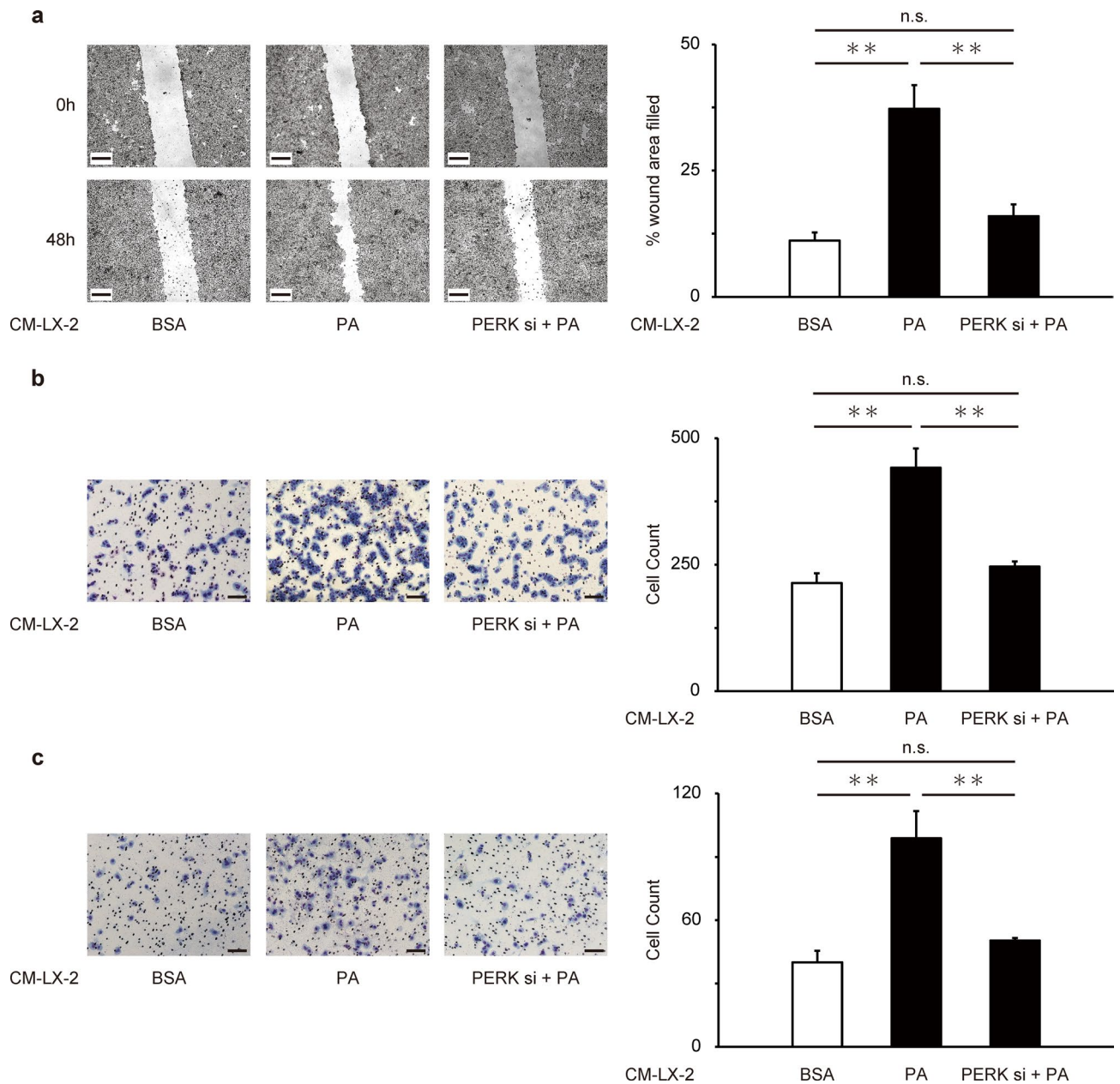
Fig. 5. PA-treated HSCs enhance HCC cell migration and invasion. The migration of HepG2 cells cultured in CM from LX-2 cells under different conditions is evaluated using scratch assay. All representative images of the scratch assay are presented in (**a**) (n = 4). Scale bar, 100 μm. Transwell assay is performed to assess the migration and invasion of HepG2 cells cultured in CM from LX-2 cells under different conditions. Migration and invasion are assessed using control and Matrigel-coated inserts, respectively. The representative images of migration and invasion cells are shown in (**b**) and (**c**), respectively (n = 4). Scale bar, 100 μm. Data are shown as the mean ± SE. Statistical analysis is performed using one-way ANOVA followed by Tukey's multiple comparison test. *$p < 0.05$, **$p < 0.01$. *Abbreviations*: PERK, protein kinase R-like endoplasmic reticulum kinase; IL-1β, interleukin-1 beta; siRNA, small interfering RNA; HSCs, hepatic stellate cells; SE, standard error; PA, palmitic acid; ANOVA, analysis of variance; BSA, bovine serum albumin; CM, conditioned medium; HCC, hepatocellular carcinoma; n.s., not significant.

knockout mice survived without developmental abnormalities compared to p38α MAPK[36], and its tissue-specific biological effects have been highlighted as a potential drug target. p38δ MAPK has also been implicated in inflammatory diseases and cancers. For example, p38δ MAPK promotes colorectal tumorigenesis via the production of inflammatory cytokines, including IL-1β, in colitis-associated colon cancer[26] and enhances tumor growth and metastasis in gastric and breast cancers[37,38]. Patients with HCC with low p38δ MAPK mRNA expression had a better prognosis than those with high p38δ MAPK mRNA expression[39]. HCC is closely
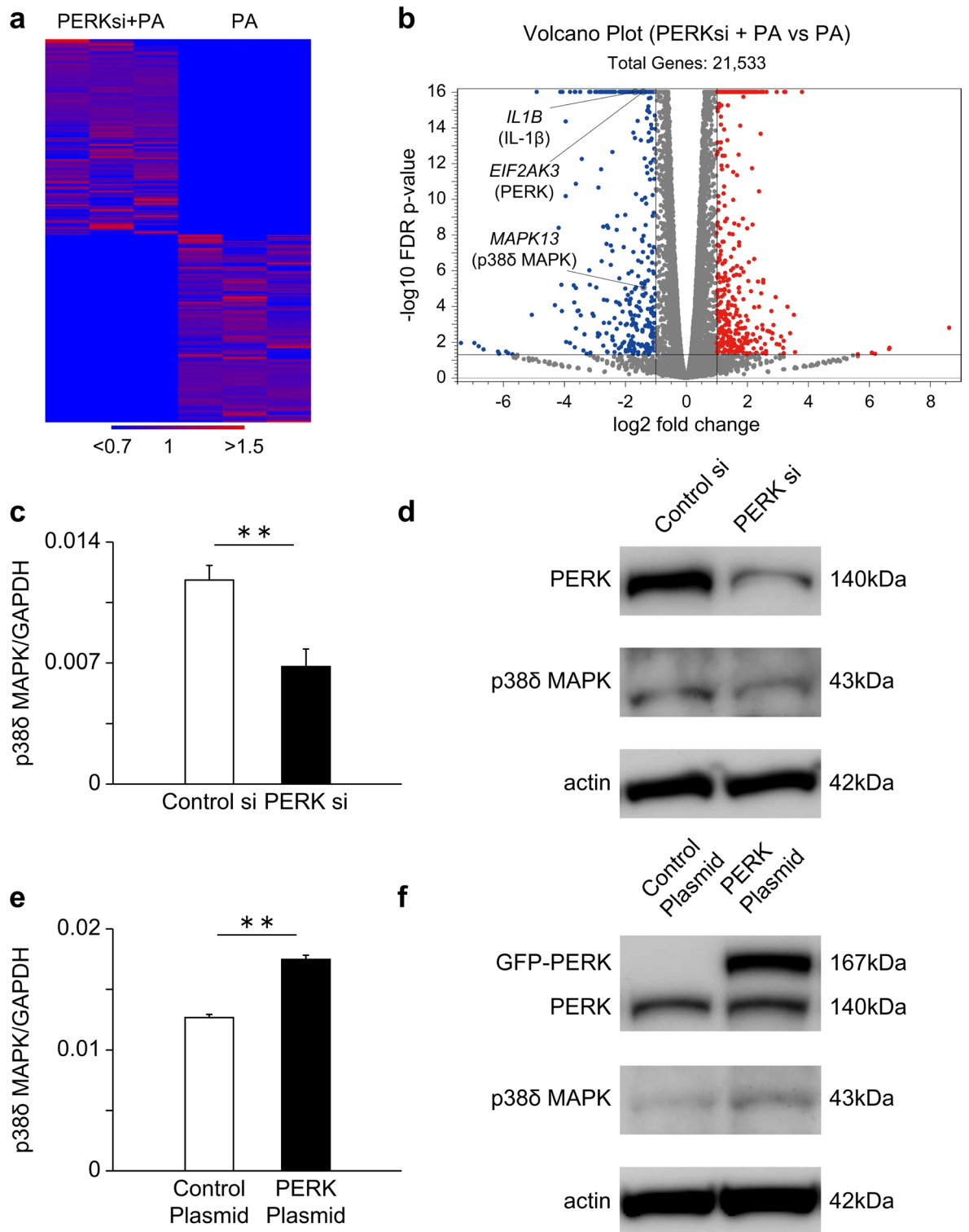
related to chronic inflammation in the liver, and p38δ MAPK may promote HCC progression by upregulating inflammatory cytokines, including IL-1β, in the TME.

IL-1β is an inflammatory cytokine that contributes to the progression of various cancer types. Its expression was higher at the tumor site than at the non-tumor site in the liver of HCC model mice[40]. Patients with HCC with higher IL-1β expression had a poorer prognosis than those with low IL-1β expression[41]; therefore, elucidating the mechanism of IL-1β production in the TME of HCC is crucial for improving HCC prognosis.

PERK inhibitors suppress ER stress-induced gene transcription and are expected to have high therapeutic efficacy; however, their clinical application may be difficult due to possible adverse events, such as pancreatic toxicity and osteogenesis imperfecta[42,43]. However, p38δ MAPK or IL-1β inhibition may be a promising therapeutic approach against HCC. AD80, which inhibits p38δ and p38γ MAPKs, was shown to be more effective than sorafenib in terms of survival rate and tumor reduction in the HCC xenograft mouse model[39]. The

◄**Fig. 6.** PERK regulates p38δ MAPK expression in HSCs. RNA-sequencing analysis is performed using the RNAs collected from PA-treated LX-2 cells and PERK siRNA-transfected PA-treated LX-2 cells. DEGs between PA (n = 3) and PERK siRNA + PA (n = 3) are determined using CLC Genomics Workbench v24. The mRNAs with a fold change > 2 and FDR p-value < 0.05 between the two groups are selected as DEGs. (**a**) DEGs are visualized using the heatmap. (**b**) Volcano plots show that *EIF2AK3* (PERK), *IL1B* (IL-1β), and *MAPK13* (p38δ MAPK) are markedly downregulated in PERK siRNA + PA compared to PA. Furthermore, p38δ MAPK expression is examined in PERK-knockdown and PERK-overexpression LX-2 cells. (**c**) p38δ MAPK mRNA (**c**) and protein (**d**) expression are evaluated using RT-PCR (n = 4) and WB, respectively. Supplementary Fig. S8 presents the original membranes of WB. p38δ MAPK mRNA (**e**) and protein (**f**) expression are evaluated using RT-PCR (n = 4) and WB, respectively. Supplementary Fig. S9 shows the original membranes of WB. Data are presented as the mean ± SE. Statistical analysis is performed using Student's *t*-test. **$p < 0.01$. *Abbreviations*: PERK, protein kinase R-like endoplasmic reticulum kinase; IL-1β, interleukin-1 beta; MAPK, mitogen-activated protein kinase; GAPDH, glyceraldehyde 3-phosphate dehydrogenase; WB, western blotting; RT, reverse transcription; siRNA, small interfering RNA; HSCs, hepatic stellate cells; SE, standard error; PA, palmitic acid; DEGs, differentially expressed genes; FDR, false discovery rate.
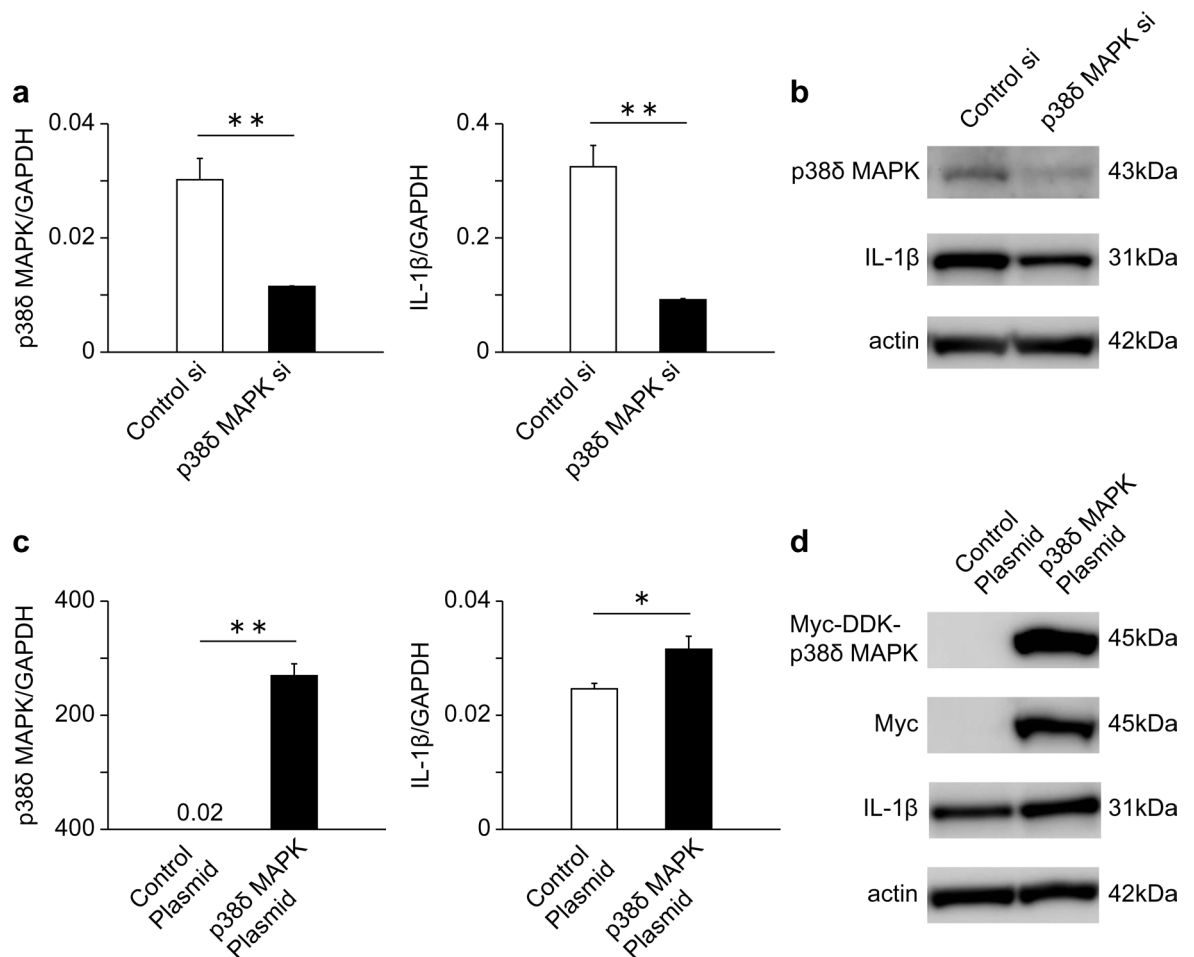

Fig. 7. p38δ MAPK regulates IL-1β expression in HSCs. p38δ MAPK knockdown is performed in LX-2 cells using siRNA, and the expression of p38δ MAPK and IL-1β is verified. (**a**) The mRNA expression of p38δ MAPK and IL-1β are evaluated using RT-PCR (n = 4). (**b**) p38δ MAPK and IL-1β protein expression are determined by WB. Supplementary Fig. S10 presents the original membranes of WB. p38δ MAPK is overexpressed in LX-2 cells using a plasmid, and the expression of p38δ MAPK and IL-1β is assessed. (**c**) p38δ MAPK and IL-1β mRNA expression are evaluated using RT-PCR (n = 4). (**d**) p38δ MAPK and IL-1β protein expression are determined using WB. Supplementary Fig. S11 presents the original membranes of WB. Data are shown as the mean ± SE. Statistical analysis is performed using Student's *t*-test. *$p < 0.05$, **$p < 0.01$. *Abbreviations*: IL-1β, interleukin-1 beta; MAPK, mitogen-activated protein kinase; GAPDH, glyceraldehyde 3-phosphate dehydrogenase; WB, western blotting; RT, reverse transcription; siRNA, small interfering RNA; HSCs, hepatic stellate cells; SE, standard error.

antibody and receptor antagonist targeting IL-1β inhibited HCC metastasis in vivo[24]. In this study, we confirmed that IL-1β NAb suppressed the proliferation of HCC cells cultured in CM from PA-treated HSCs.

Based on our findings and on previous reports, the PERK/IL-1β axis represents a promising therapeutic target in MASH-related HCC. In this study, we demonstrated using in vitro experiments that IL-1β secretion in HSCs is dependent on PERK expression. In addition, previous studies have shown that PERK is activated and IL-1β expression is upregulated in MASH model mice[44,45]. Because IL-1β has been shown to promote HCC progression in vitro, it is plausible that the PERK/IL-1β axis plays a crucial role in the progression of MASH-related HCC. This axis represents a novel therapeutic target and may serve as an effective treatment strategy, especially for patients with MASH-related HCC who exhibit resistance to existing therapies, including immunotherapy.

Considering these findings, a potential future research direction aimed at therapeutic applications targeting the PERK/p38δ MAPK/IL-1β axis in HSCs would be to evaluate whether the administration of IL-1β NAb can suppress tumor growth and metastasis in a xenograft model transplanted with PA-treated HSCs and HCC cells.

This study has some limitations. First, our findings are primarily based on in vitro experiments and therefore require validation in in vivo models such as high-fat diet-fed mice. Additionally, immunohistochemical staining could serve as a useful approach for investigating the expression of PERK and IL-1β in HSCs in MASH-related HCC. Second, our findings are based on RNA-seq analysis combined with siRNA-based and plasmid-based functional experiments. The incorporation of multi-modal data-integration approaches could further enhance the reproducibility of our findings.

In conclusion, our study revealed that PERK in HSCs promotes HCC progression via the p38δ MAPK/IL-1β axis (Fig. 8). This axis may be a novel therapeutic approach for MASH-related HCC, where ER stress markedly contributes to the pathogenesis.

Methods

Cell culture
LX-2 cells, a human HSC cell line from Merck (Darmstadt, Germany), were cultured in Dulbecco's modified Eagle medium (DMEM) free of glutamine (Thermo Fisher Scientific, Waltham, MA, USA) containing 2% fetal bovine serum (FBS) (Thermo Fisher Scientific), 2 mM L-Glutamine (Thermo Fisher Scientific), and 1% penicillin and streptomycin. HepG2 cells, a human HCC cell line obtained from the Japanese Collection of Research Bioresources (Osaka, Japan), were grown in DMEM (Thermo Fisher Scientific) containing 10% FBS and 1% penicillin and streptomycin. Both cells were incubated at 37 °C in a 5% CO_2 humidified incubator.

Preparation of PA
Approximately 0.0256 g of PA was dissolved in 1 mL of 99% ethanol, followed by 2.0 g of fatty acid-free BSA added to 18 mL of sterile water, along with 160 μL of 1 N NaOH. The BSA solution was sterilized using a 0.22-μm filter. Finally, the PA and sterilized BSA solutions were heated at 50 °C for 2 min, and approximately 100 μL of the PA solution was added to 900 μL of the BSA solution. Because PA was dissolved in a BSA solution for solubilization, BSA-treated cells were used as the vehicle control.

RNA interference
We used PERK (UAG CAA AUC UUC UGA A), p38δ MAPK (GCU CAA AGG CCU UAA GUA C), and control (Dharmacon, Cambridge, UK) siRNAs. LX-2 cells at 60% confluence in six-well plates were transfected with 12.25 nM siRNA using RNAiMAX (Thermo Fisher Scientific). Approximately 24 h after transfection, the RNAs and proteins were isolated from the cells.

PERK and p38δ MAPK plasmids
PERK (RG214993) and p38δ MAPK (RC200606) plasmids were obtained from Origene (Rockville, MD), and pCMV6 was used as the control plasmid. LX-2 cells at 70% confluence were transfected with 0.25 μg/mL plasmid using Lipofectamine LTX (Thermo Fisher Scientific). The RNAs and proteins were isolated from the cells approximately 24 h after transfection.

RNA extraction, cDNA synthesis, and real-time reverse transcription-PCR
RNA extraction and RT were performed using RNeasy Plus Mini Kit (Qiagen, Venlo, Netherlands) and a High-Capacity cDNA Reverse Transcription Kit (Thermo Fisher Scientific), respectively. Target gene-specific primers were used for PCR amplification. Real-time PCR was performed using LightCycler LC480 (Roche Diagnostics, Rotkreuz, Switzerland) and SYBR Green I dye (Roche Diagnostics). For each experimental group, four biological replicates (n = 4) were analyzed, with technical duplicates for each sample. mRNA expression was normalized to glyceraldehyde 3-phosphate dehydrogenase mRNA and subsequently analyzed statistically. The primers employed for PCR are provided in Supplementary Table S2.

Western blotting
Protein extraction was performed using radio-immunoprecipitation assay buffer (10 mM Tris–HCl, 1% sodium dodecyl sulfate, 0.5% NP-40, 150 mM NaCl, and pH 7.4). Briefly, 20 μg of protein was loaded per lane onto 4–12% Bis–Tris Plus gels (Thermo Fisher Scientific) and transferred to Immobilon-P membranes (Millipore, Bedford, MA, USA). The membranes were incubated overnight at 4 °C with primary antibodies that bind to target proteins and subsequently incubated with secondary antibodies for 1 h at room temperature. Protein bands were visualized using the Enhanced Chemiluminescence (ECL) Prime kit (Cytiva, Tokyo, Japan) and ImageQuant LAS 4000 (GE Healthcare, Chicago, IL, USA) or Amersham ImageQuant 800 (Cytiva). The primary and secondary antibodies used for WB are specified in Supplementary Table S3.
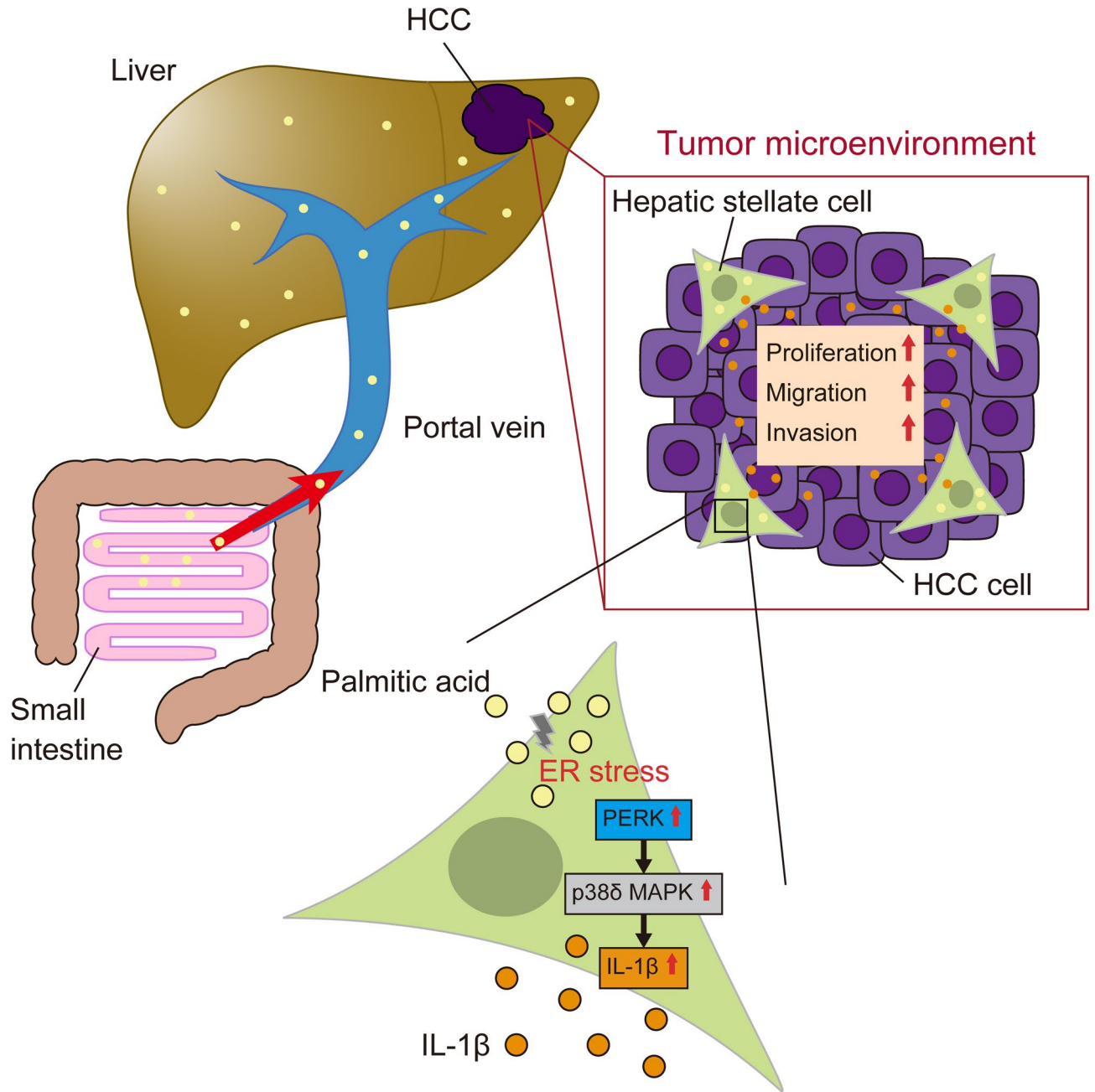
Fig. 8. PERK in HSCs promotes HCC progression via the p38δ MAPK/IL-1β axis. In the tumor microenvironment of MASH-related HCC, PA absorbed from the intestine induces ER stress in HSCs, activating PERK signaling. PERK subsequently promotes IL-1β secretion via the p38δ MAPK/IL-1β axis, enhancing the proliferation, migration, and invasion of HCC cells, thereby contributing to HCC progression. *Abbreviations*: MASH, metabolic dysfunction-associated steatohepatitis; HCC, hepatocellular carcinoma; HSCs, hepatic stellate cells; ER, endoplasmic reticulum; PERK, protein kinase R-like endoplasmic reticulum kinase; IL-1β, interleukin-1 beta; MAPK, mitogen-activated protein kinase; PA, palmitic acid.

Collection of CM

LX-2 cells were seeded into six-well plates at a density of 1.8×10^5 cells per well to collect the CM. Control or PERK siRNA transfection was performed the following day. After 24 h, the cells were treated with BSA control or PA (20 μM) for another 24 h. The culture medium was replaced with a serum-free medium post-treatment. After 24 h, the cell supernatant was collected and centrifuged at 1000 rpm for 15 min to remove the cell debris. The supernatant was harvested as the CM and preserved at −80 °C.

Enzyme-linked immunosorbent assay

The enzyme-linked immunosorbent assay kit (R&D Systems, Minneapolis, MN, USA) was used to measure the IL-1β concentration in the CM from LX-2 cells, following the manufacturer's instructions. Measurements were performed using four biological replicates per group (n = 4), with technical duplicates for each sample.

Proliferation assay

HepG2 cells were seeded into 96-well flat-bottom plates at a density of 5×10^3 cells/well in serum-free medium and incubated for 24 h. Subsequently, the cells were subjected to different treatments. For IL-1β treatment, rhIL-1β (R&D Systems) was added to each well at final concentrations of 10, 100, and 1000 pg/mL, with PBS as a control. The culture medium was replaced with 100 μL of CM from LX-2 cells under different conditions for CM treatment. Regarding the IL-1β neutralization assay, the culture medium was replaced with CM from PA-treated LX-2 cells, followed by the addition of an IL-1β NAb (10, 100, and 1000 ng/mL; InvivoGen, San Diego, CA, USA) or control antibody (InvivoGen). Cell proliferation was assessed at 0, 24, 48, and 72 h after treatment using the MTS assay. Finally, the cells were incubated for 1 h after the addition of the MTS reagent (Promega, Fitchburg, WI, USA), and the absorbance was measured at 450 nm. All experimental conditions were evaluated using six biological replicates per group (n = 6).

Scratch assay

HepG2 cells were seeded into six-well plates at a density of 2×10^5 cells/well and cultured in DMEM containing 10% FBS. The cell layer was scratched with a 200-μL pipette tip once the cell confluence reached 90–100%, and the supernatant was replaced with 2 mL of the CM from LX-2 cells under different conditions. Images were captured at 0 and 48 h after scratching, at a 50× magnification, using a microscope (ZEISS Axio Vert.A1; Carl Zeiss, Oberkochen, Germany). The change in the wound area was calculated using the following formula: $\{(wound\ area\ at\ 0\ \mathrm{h} - wound\ area\ at\ 48\ \mathrm{h})\ /wound\ area\ at\ 0\ \mathrm{h}\} \times 100\ (\%)$. ImageJ Software (National Institutes of Health, Bethesda, MD, USA) was used to measure the wound area. The assay was performed using four biological replicates per group (n = 4).

Transwell assay

A Transwell assay was performed to evaluate the effects of the CM from LX-2 cells under different conditions on HepG2 cell migration and invasion. For the migration assay, HepG2 cells suspended in serum-free medium were seeded into the upper chamber of the Transwell (8 μm pore size, Corning, MA, USA) at a density of 1×10^5 cells/well. Approximately 750 μL of the CM from LX-2 cells under different conditions was added to the lower chamber, and the cells were incubated at 37 °C. After 48 h, the cells remaining on the inside of the upper chamber were removed with cotton swabs. Those on the lower surface were stained with Diff-Quik staining (Sysmex Corporation, Hyogo, Japan) and counted under a microscope in four random fields at 100× magnification. The upper chamber coated with Matrigel (Corning, MA, USA) was used for the invasion assay. All other procedures were performed as described for the migration assay. Migration and invasion assays were each conducted using four biological replicates per group (n = 4).

RNA-sequencing analysis

To investigate genes upregulated by PA treatment but suppressed by PERK knockdown, we used RNA samples from PA-treated cells and PA-treated cells with PERK knockdown. Total RNA was obtained from PA-treated LX-2 cells and PERK siRNA-transfected PA-treated LX-2 cells, with three biological replicates (n = 3) prepared for each group. The integrity of the total RNA (RIN) was evaluated using an Agilent 2100 Bioanalyzer (Agilent Technologies, Santa Clara, CA, USA). We used the samples with a RIN value > 9 and constructed RNA-sequencing (RNA-seq) libraries using the NEBNext Ultra II Directional RNA Library Prep Kit for Illumina (New England BioLabs; NEB, Ipswich, MA, USA). Sequencing of single reads (75 bp) was performed with the NextSeq 500/550 High Output Kit v2.5 (75 Cycles) on NextSeq500 (Illumina, San Diego, CA, USA). Sequence data were analyzed using CLC Genomics Workbench v24 (QIAGEN, Hilden, Germany) with default settings. Briefly, the FASTQ files were trimmed and subsequently mapped on the human genome data of hg38. Significant DEGs were detected based on TMM normalization and a negative binomial Generalized Linear Model (GLM). Low-expression genes across all groups were filtered prior to false discovery rate (FDR) correction. DEGs between the PA group and the PERK siRNA + PA group were determined. Finally, the mRNAs with a fold change > 2 and an FDR p-value < 0.05 between the two groups were selected as DEGs.

Statistical analysis

All statistical analyses were performed using R version 4.4.0 (R Foundation for Statistical Computing, Vienna, Austria). Quantitative data are presented as the mean ± standard error of the mean (SEM; calculated by dividing the standard deviation by the square root of the number of biological replicates in each group). To evaluate differences between two groups, Student's t-test was applied under the assumption of normally distributed data with equal variances. For comparisons involving more than two groups, one-way analysis of variance (ANOVA) was performed to assess overall differences among group means. When ANOVA indicated a significant difference, Tukey's multiple comparison test was used for post hoc pairwise comparisons to determine which specific groups differed. Prior to these analyses, the Shapiro–Wilk test was used to assess normality. Homogeneity of variances was verified using the F-test for comparisons between two groups and Bartlett's test for comparisons among three groups. All data used in the parametric tests satisfied these assumptions. A p-value of < 0.05 was considered statistically significant.

Data availability

The datasets generated and/or analyzed during the current study are available in the Gene Expression Omnibus (GEO) repository, GSE292002 and are available from the corresponding author on reasonable request.

References

1. Sung, H. et al. Global cancer statistics 2020: GLOBOCAN estimates of incidence and mortality worldwide for 36 cancers in 185 countries. *CA Cancer J. Clin.* **71**, 209–249 (2021).
2. Tateishi, R. et al. A nationwide survey on non-B, non-C hepatocellular carcinoma in Japan: 2011–2015 update. *J. Gastroenterol.* **54**, 367–376 (2019).
3. Younossi, Z. M. et al. The global epidemiology of nonalcoholic fatty liver disease (NAFLD) and nonalcoholic steatohepatitis (NASH): A systematic review. *Hepatology* **77**, 1335–1347 (2023).
4. Estes, C. et al. Modeling NAFLD disease burden in China, France, Germany, Italy, Japan, Spain, United Kingdom, and United States for the period 2016–2030. *J. Hepatol.* **69**, 896–904 (2018).
5. Pfister, D. et al. NASH limits anti-tumour surveillance in immunotherapy-treated HCC. *Nature* **592**, 450–456 (2021).
6. Llovet, J. M. et al. Hepatocellular carcinoma. *Nat. Rev. Dis. Primers* **7**, 6 (2021).
7. Hernandez-Gea, V., Toffanin, S., Friedman, S. L. & Llovet, J. M. Role of the microenvironment in the pathogenesis and treatment of hepatocellular carcinoma. *Gastroenterology* **144**, 512–527 (2013).
8. Yang, J. D., Nakamura, I. & Roberts, L. R. The tumor microenvironment in hepatocellular carcinoma: current status and therapeutic targets. *Semin. Cancer Biol.* **21**, 35–43 (2011).
9. Li, S. et al. Hepatic stellate cell-released CXCL1 aggravates HCC malignant behaviors through the MIR4435-2HG/miR-506-3p/TGFB1 axis. *Cancer Sci.* **114**, 504–520 (2023).
10. Iwahasi, S. et al. Hepatic stellate cells contribute to the tumor malignancy of hepatocellular carcinoma through the IL-6 pathway. *Anticancer Res.* **40**, 743–749 (2020).
11. Friedman, S. L. Hepatic stellate cells: protean, multifunctional, and enigmatic cells of the liver. *Physiol. Rev.* **88**, 125–172 (2008).
12. Wake, K. "Sternzellen" in the liver: perisinusoidal cells with special reference to storage of vitamin A. *Am. J. Anat.* **132**, 429–462 (1971).
13. Weiskirchen, R. Hepatoprotective and anti-fibrotic agents: it's time to take the next step. *Front. Pharmacol.* **6**, 303 (2016).
14. Ho, C. H. et al. Wild bitter melon extract regulates LPS-induced hepatic stellate cell activation, inflammation, endoplasmic reticulum stress, and ferroptosis. *Evid. Based Complement. Alternat. Med.* **2021**, 6671129. https://doi.org/10.1155/2021/6671129 (2021).
15. Wang, M., Li, L., Xu, Y., Du, J. & Ling, C. Roles of hepatic stellate cells in NAFLD: from the perspective of inflammation and fibrosis. *Front. Pharmacol.* **13**, 958428. https://doi.org/10.3389/fphar.2022.958428 (2022).
16. Higashi, T., Friedman, S. L. & Hoshida, Y. Hepatic stellate cells as key target in liver fibrosis. *Adv. Drug Deliv. Rev.* **121**, 27–42 (2017).
17. Tilg, H., Adolph, T. E., Dudek, M. & Knolle, P. Non-alcoholic fatty liver disease: the interplay between metabolism, microbes and immunity. *Nat. Metab.* **3**, 1596–1607 (2021).
18. Hanayama, M. et al. The mechanism of increased intestinal palmitic acid absorption and its impact on hepatic stellate cell activation in nonalcoholic steatohepatitis. *Sci. Rep.* **11**, 13380. https://doi.org/10.1038/s41598-021-92790-z (2021).
19. Imai, Y. *et al.* Stimulated hepatic stellate cell promotes progression of hepatocellular carcinoma due to protein kinase R activation. *PLOS One* **14**, e0212589; https://doi.org/10.1371/journal.pone.0212589 (2019).
20. Cao, J. et al. Saturated fatty acid induction of endoplasmic reticulum stress and apoptosis in human liver cells via the PERK/ATF4/CHOP signaling pathway. *Mol. Cell. Biochem.* **364**, 115–129 (2012).
21. Ando, T. et al. GSK2656157, a PERK inhibitor, reduced LPS-induced IL-1β production through inhibiting caspase 1 activation in macrophage-like J774.1 cells. *Immunopharmacol. Immunotoxicol.* **38**, 298–302 (2016).
22. Wang, A. et al. Endoplasmic reticulum stress-related super enhancer promotes epithelial-mesenchymal transformation in hepatocellular carcinoma through CREB5 mediated activation of TNC. *Cell Death Dis.* **16**, 73. https://doi.org/10.1038/s41419-025-07356-y (2025).
23. Kopsida, M. et al. Inhibiting the endoplasmic reticulum stress response enhances the effect of doxorubicin by altering the lipid metabolism of liver cancer cells. *Mol. Metab.* **79**, 101846. https://doi.org/10.1016/j.molmet.2023.101846 (2024).
24. Gao, Z. et al. Inhibition of autophagy in macrophage promotes IL-1β-mediated hepatocellular carcinoma progression via inflammasome accumulation and self-recruitment. *Biomed. Pharmacother.* **161**, 114560. https://doi.org/10.1016/j.biopha.2023.114560 (2023).
25. Risco, A. et al. p38γ and p38δ kinases regulate the Toll-like receptor 4 (TLR4)-induced cytokine production by controlling ERK1/2 protein kinase pathway activation. *Proc. Natl Acad. Sci. USA* **109**, 11200–11205 (2012).
26. Del Reino, P. et al. Pro-oncogenic role of alternative P38 mitogen-activated protein kinases p38γ and p38δ, linking inflammation and cancer in colitis-associated colon cancer. *Cancer Res.* **74**, 6150–6160 (2014).
27. Wu, M., Miao, H., Fu, R., Zhang, J. & Zheng, W. Hepatic stellate cell: a potential target for hepatocellular carcinoma. *Curr. Mol. Pharmacol.* **13**, 261–272 (2020).
28. Wei, J. & Fang, D. Endoplasmic reticulum stress signaling and the pathogenesis of hepatocarcinoma. *Int. J. Mol. Sci.* **22**, 1799. https://doi.org/10.3390/ijms22041799 (2021).
29. Koo, J. H., Lee, H. J., Kim, W. & Kim, S. G. Endoplasmic reticulum stress in hepatic stellate cells promotes liver fibrosis via PERK-mediated degradation of HNRNPA1 and up-regulation of SMAD2. *Gastroenterology* **150**, 181-193.e8 (2016).
30. Xue, F. et al. Coordinated signaling of activating transcription factor 6alpha and inositol-requiring enzyme 1alpha regulates hepatic stellate cell-mediated fibrogenesis in mice. *Am. J. Physiol. Gastrointest. Liver Physiol.* **320**, G864–G879 (2021).
31. Liu, Z. et al. Transforming growth factor β (TGFβ) cross-talk with the unfolded protein response is critical for hepatic stellate cell activation. *J. Biol. Chem.* **294**, 3137–3151 (2019).
32. Pavlović, N. et al. Inhibiting IRE1alpha-endonuclease activity decreases tumor burden in a mouse model for hepatocellular carcinoma. *Elife* **9**, e55865. https://doi.org/10.7554/eLife.55865 (2020).
33. Cuenda, A. et al. SB 203580 is a specific inhibitor of a MAP kinase homologue which is stimulated by cellular stresses and interleukin-1. *FEBS Lett.* **364**, 229–233 (1995).
34. Adams, R. H. et al. Essential role of p38α MAP kinase in placental but not embryonic cardiovascular development. *Mol. Cell* **6**, 109–116 (2000).
35. Anton, D. B., Ducati, R. G., Timmers, L. F. S. M., Laufer, S. & Goettert, M. I. A special view of what was almost forgotten: p38δ MAPK. *Cancers* **13**, 2077. https://doi.org/10.3390/cancers13092077 (2021).
36. Sumara, G. et al. Regulation of PKD by the MAPK p38δ in insulin secretion and glucose homeostasis. *Cell* **136**, 235–248 (2009).
37. Shi, D. B. et al. GAGE7B promotes tumor metastasis and growth via activating the p38δ/pMAPKAPK2/pHSP27 pathway in gastric cancer. *J. Exp. Clin. Cancer Res.* **38**, 124 (2019).

38. Wada, M. et al. P38 delta MAPK promotes breast cancer progression and lung metastasis by enhancing cell proliferation and cell detachment. *Oncogene* **36**, 6649–6657 (2017).
39. Yu, J. X. et al. Phenotype-based screens with conformation-specific inhibitors reveal p38 gamma and delta as targets for HCC polypharmacology. *Mol. Cancer Ther.* **18**, 1506–1519 (2019).
40. Chu, C. S. et al. Interleukin-1 receptor 1 deficiency worsens hepatocellular carcinoma, while gemcitabine treatment alleviates the hepatocellular carcinoma-induced increase in intra-hepatic immune cells. *J. Gastroenterol. Hepatol.* **39**, 2208–2218 (2024).
41. Zhang, J. et al. Hypoxia-inducible factor-1α/interleukin-1β signaling enhances hepatoma epithelial-mesenchymal transition through macrophages in a hypoxic-inflammatory microenvironment. *Hepatology* **67**, 1872–1889 (2018).
42. Wei, J., Sheng, X., Feng, D., McGrath, B. & Cavener, D. R. PERK is essential for neonatal skeletal development to regulate osteoblast proliferation and differentiation. *J. Cell. Physiol.* **217**, 693–707 (2008).
43. Yu, Q. et al. Type I interferons mediate pancreatic toxicities of PERK inhibition. *Proc. Natl Acad. Sci. USA* **112**, 15420–15425 (2015).
44. Bandla, H. et al. Deletion of endoplasmic reticulum stress-responsive co-chaperone p58IPK protects mice from diet-induced steatohepatitis. *Hepatol Res.* **48**, 479–494 (2018).
45. Kamari, Y. et al. Lack of interleukin-1α or interleukin-1β inhibits transformation of steatosis to steatohepatitis and liver fibrosis in hypercholesterolemic mice. *J. Hepatol.* **55**, 1086–1094 (2011).

Acknowledgements

Author contributions

All authors contributed to the study's conception and design. Material preparation, experiments, data collection and analysis were performed by M.M., Y.T., T.W., and Y.I.. M.M. and Y.T. wrote the manuscript. All authors read and approved the final manuscript.

Funding

Declarations

Competing interests

The authors declare no competing interests.

Ethical approval

Not applicable.

Informed consent

Not applicable.

Additional information

Supplementary Information The online version contains supplementary material available at https://doi.org/10.1038/s41598-025-04150-w.

Correspondence and requests for materials should be addressed to Y.T.

Reprints and permissions information is available at www.nature.com/reprints.

Publisher's note Springer Nature remains neutral with regard to jurisdictional claims in published maps and institutional affiliations.